HHS Public Access

Author manuscript

J Neurosci Methods. Author manuscript; available in PMC 2021 December 01.

Published in final edited form as:

J Neurosci Methods. 2020 December 01; 346: 108926. doi:10.1016/j.jneumeth.2020.108926.

Novel proton exchange rate MRI presents unique contrast in brains of ischemic stroke patients

Zhenxiong Wang[a,b], **Mehran Shaghaghi**[b], **Shun Zhang**[a], **Guiling Zhang**[a], **Yiran Zhou**[a], **Di Wu**[a], **Zhuoli Zhang**[c], **Wenzhen Zhu**[a,*], **Kejia Cai**[b,*]

[a]Department of Radiology, Tongji Hospital, Tongji Medical College, Huazhong University of Science and Technology, Wuhan, China

[b]Departments of Radiology, Department of Bioengineering, and the Center for MR Research, University of Illinois at Chicago, Chicago, USA

[c]Department of Radiology, Northwestern University, Chicago , USA

Abstract

Background: To map and quantify the proton exchange rate (k_{ex}) of brain tissues using improved omega plots in ischemic stroke patients and to investigate whether k_{ex} can serve as a potential endogenous surrogate imaging biomarker for detecting the metabolic state and the pathologic changes due to ischemic stroke.

New Method: Three sets of Z-spectra were acquired from seventeen ischemic stroke patients using a spin echo-echo planar imaging sequence with pre-saturation chemical exchange saturation transfer (CEST) pulse at B_1 of 1.5, 2.5, and 3.5 μT, respectively. Pixel-wise k_{ex} was calculated from improved omega plot of water direct saturation (DS)-removed Z-spectral signals.

Results: The derived k_{ex} maps can differentiate infarcts from contralateral normal brain tissues with significantly increased signal (893 ± 52 s^{-1} vs. 739 ± 34 s^{-1}, P < 001).

Comparison with Existing Method(s): The k_{ex} maps were found to be different from conventional contrasts from diffusion-weighted imaging (DWI), CEST, and semi-solid magnetization transfer (MT) MRI. In brief, k_{ex} MRI showed larger lesion areas than DWI with different degrees and different lesion contrast compared to CEST and MT.

*Corresponding authors **Wenzhen Zhu**, Department of Radiology, Tongji Hospital, Tongji Medical College, Huazhong University of Science and Technology, No. 1095 Jiefang Avenue, Wuhan, 430030 China., Tel./fax: +86- 27-83663258; zhuwenzhen8612@163.com (W. Zhu); **Kejia Cai**, Departments of Radiology, Department of Bioengineering, and the Center for MR Research, University of Illinois at Chicago, 1747 W. Roosevelt Road, Chicago, IL, 60608 USA., Tel./fax: +1- 312-413-0091; kcai@uic.edu (K. Cai).

Credit Author Statement

Zhenxiong Wang: Conceptualization, Data curation, Formal analysis, Investigation, Methodology, Roles/Writing-original draft, Writing-review & editing. **Mehran Shaghaghi:** Formal analysis, Investigation, Methodology, Software, Writing-review & editing. **Shun Zhang:** Data curation, Investigation, Methodology, Writing - review & editing. **Guiling Zhang:** Data curation, Methodology, Investigation, Writing-review & editing. **Yiran Zhou:** Data curation, Investigation, Writing-review & editing. **Di Wu:** Data curation, Investigation, Writing-review & editing. **Zhuoli Zhang:** Methodology, Software, Writing-review & editing. **WenzhenZhu:** Conceptualization, Data curation, Formal analysis, Funding acquisition, Methodology, Project administration, Resources, Supervision, Writing-review & editing. **Kejia Cai:** Conceptualization, Data curation, Formal analysis, Funding acquisition, Methodology, Project administration, Resources, Supervision, Roles/Writing-original draft, Writing-review & editing.

Conclusions: In this preliminary translational research, the k_{ex} MRI based on DS-removed omega plots has been demonstrated for *in vivo* imaging of clinical ischemic stroke patients. As a noninvasive and unique MRI contrast, k_{ex} MRI at 3T may serve as a potential surrogate imaging biomarker for the metabolic changes of stroke and help for monitoring the evolution and the treatment of stroke.

Graphical abstract

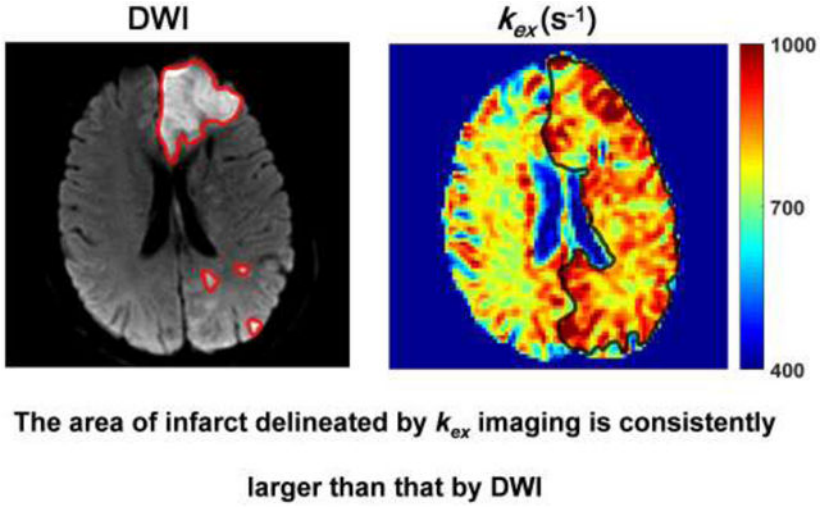

Keywords

chemical exchange saturation transfer (CEST); omega plot; proton exchange rate (k_{ex}); stroke

1 Introduction

The search for novel and robust noninvasive molecular imaging techniques to accurately detect the metabolic disturbances of ischemic brain tissues is currently ongoing. Unlike the stroke during the hyperacute or acute phase, the subacute and chronic phases provide an adequate window for evaluating novel imaging techniques. In addition, through assessing microstructural and metabolic changes due to ischemia, MRI techniques can not only help to investigate the secondary clinical symptoms but also monitor the curative effects and predict the prognosis of the patients under subacute and chronic phases in clinics[1-4].

As an emerging endogenous metabolic MRI technique, chemical exchange saturation transfer (CEST) has shown advantages in the metabolic assessment of stroke[5-7]. Proton exchange is the fundamental contrast mechanism for CEST MRI and the *in vivo* imaging of proton exchange rate (k_{ex}) has not been achieved until recently[8,9]. Particularly, *in vivo* k_{ex} imaging of healthy brains has been demonstrated based on water direct saturation (DS) removed omega plots[8,10].

The omega plot was initially evaluated in a phantom and has shown the capacity of assessing proton exchange rate from paramagnetic CEST agents[10]. The resonance frequencies of labile protons in paramagnetic agents are far from the water resonance and hence their

signals are negligibly affected by the water DS effect. However, the saturation offsets of exchangeable protons in endogenous diamagnetic CEST metabolites in biological tissues are close to the water proton resonance[11,12]. Hence, the water DS effect is a dominant confounding factor contributing to the Z-spectral signal during *in vivo* imaging[13,14]. Mathematical removal of the water DS signal has been used to eliminate the predominant contamination by the DS effect for the quantification of k_{ex} *in vivo*[8]. Our previous study using DS-removed omega plots has shown that the exchange rate maps can linearly reflect the pH changes in the physiological range (pH 6.2 to 7.4) for *ex vivo* protein solutions[8].

The purpose of this study was to investigate the changes of k_{ex} in ischemic brain tissues of subacute and chronic stroke patients based on the DS-removed omega plots and to evaluate the potential value of k_{ex} imaging in the detection of physiopathologic changes in ischemic stroke under clinical settings.

2 Methods

2.1 Patients

The study was approved by the institutional ethics committee and written informed consent was obtained from each participant prior to the examination. A total of 23 patients with ischemic stroke (16 men, 7 women, mean age 56 years, age range 32–81 years, duration of stroke onset from 2 to 18 days) were recruited from December 2018 to April 2019 in this prospective study. The inclusion criteria included suspected symptoms of ischemic stroke and explicit infarcts observed on CT or MRI. Lesions were consistent with symptoms and arterial distribution, showing low density in CT, or high signal in diffusion-weighted imaging (DWI) and T2-weighted fluid-attenuated inversion recovery (T2-FLAIR), low signal in T1-weighted fluid-attenuated inversion recovery (T1-FLAIR). Exclusion criteria included hemorrhagic transformation detected by CT or T1-FLAIR, bilateral hemispheric infarcts, insufficient image quality, other nervous disorders, and all contraindications to MRI. Of these patients, 6 excluded because of hemorrhagic transformation (n = 1), bilateral hemispheric infarcts (n = 2), and motion artifacts (n = 3). Thus, 17 cases were included for the final analysis.

2.2 Image acquisition

All MRI examinations were performed on a 3T MRI system (GE Medical Systems, Discovery MR750, Waukesha, WI, USA) with a 32-channel head coil. Several routine MRI protocols were used for localizing the infarct and excluding any other lesions, including transverse T1-FLAIR, T2-FLAIR, and DWI based on spin-echo echo-planar imaging (SE-EPI) sequence.

After the anatomical slice selection, single-slice Z-spectral data were acquired on a transverse section crossing the largest infarct region in reference to DWI using a SE-EPI sequence. The detailed parameters were as follows: repetition time (TR) = 3000 ms, echo time (TE) = 22.6 ms, matrix size = 128×128, field of view = 240 mm × 240 mm, slice thickness = 5 mm, CEST saturation power (B_1) was set to 1.5, 2.5 and 3.5 μT, saturation duration = 1500 ms, a total 33 saturation offsets including 0 to ±5 ppm at an increment of

0.25 ppm, plus ±6, +15.6, and +39.1 ppm (as reference image), and acquisition time of 3 min 18 s for each of the three Z-spectra.

2.3 Data analysis

All raw data processing and analysis were performed using home-built programs developed in MATLAB (2018a, MathWorks, Natick, MA, USA). Prior to analysis, motion artifacts in Z-spectral images were corrected based on image registration routine "imregister". All Z-spectra were B_0-corrected based on the B_0 map estimated from the Z-spectrum collected with the minimal saturation power (1.5 μT). Then the Z-spectra were flipped to be 100 × (1 − M_z/M_0), in which M_0 is the reference for Z-spectrum signal (M_z). The flipped Z-spectrum was then fitted to a linear combination of two Lorentzian functions corresponding to the bulk water and the residual signal, centered around 0 and −1.5 ppm respectively, chosen according to previous study (Cai et al., 2015). . The residual signal contains all exchanging components, including CEST, magnetization transfer (MT) from semi-solid components, and relayed nuclear overhauser enhancement (NOE)[13]. After the fitting, the bulk water peak was subtracted from the raw Z-spectra and the residual signal was used for further omega plot analysis. The omega plot was constructed as the plot of $M_z/(M_0-M_z)$ versus $1 / \omega_1^2$, where M_z & M_0 are now taken from the signals of the DS-removed spectra, and $\omega_1 = \gamma B_1$ is the amplitude of the saturation radiofrequency (RF) pulse. Linear fit to the omega plot was used to determine the X-axis intercept (typically negative). Next, the intercept value was used to calculate the average k_{ex} of all contributing metabolites according to $\frac{-1}{x_{intercept}} = k_{ex}$.

In our previous research, a more generalized equation as follows was derived in case of more than one exchanging metabolite species contributing to the saturation transfer signal[8].

$$\frac{M_z}{M_0 - M_z} = \frac{1}{T_1^w}\left(\frac{\sum_{i=1}^{n} \frac{k_{s_i}}{f_{s_i}}}{\omega_1^2} + \sum_{i=1}^{n} \frac{1}{f_{s_i} k_{s_i}}\right) \tag{1}$$

in which T_1^w is the longitudinal relaxation time of the water, k_{s_i} are the exchange rates of all metabolites' pool and the water pool and f_{s_i} are the fraction of protons on the metabolites relative to water's. Similar to the original omega plot equation, Equation 1 indicates a linear relationship between $\mathcal{Y} = \frac{M_z}{M_0 - M_z}$ and the inverse of the square of saturation pulse power, $\mathcal{X} = \frac{1}{\omega_1^2}$. This means the X-axis intercept of the $\mathcal{Y}$ *vs.* $\mathcal{X}$ plot (the omega plot) can provide a readout of the convoluted k_{ex} average of all exchanging components according to the following equation.

$$\frac{-1}{x_{intercept}} = \frac{\sum_1^n \frac{k_{s_i}}{f_i}}{\sum_1^n \frac{1}{f_i k_{s_i}}} = M_1\left(\frac{k_{s_i}}{f_i}\right) \times M^{-1}\left(f_i k_{s_i}\right) = p^2\left(f_i k_{s_i}\right) = p^2(\bar{k}_{ex}) \tag{2}$$

where M_1 and M^{-1} are the arithmetic and the harmonic mean operator, respectively.

Here, the quantified exchange rate value reflects a profile of the average exchange rate of all the contributing components and exchanging metabolites to the Z-spectral signals. Following this procedure for each pixel, the exchanging rate maps of the brains without the DS effect were then constructed.

For comparison, conventional CEST and MT maps were quantified as

$$\mathrm{CEST}_{asym} = \frac{M_z(-3.5\ ppm) - M_z(+3.5\ ppm)}{M_0} \times 100\,\% \tag{3}$$

and

$$\mathrm{MT} = (1 - \frac{M_z(+6\ ppm)}{M_0}) \times 100\,\% \tag{4}$$

Given that stroke lesions were visually differentiable from control tissues in k_{ex} images, regions of interest (ROIs) of infarcts and the corresponding contralateral healthy tissues were manually drawn in reference to k_{ex} images by a neuroradiologist (5 years of experience) and double-checked by another senior neuroradiologist (8 years of experience). There were some small hot spots in k_{ex} images that are potentially small infarct lesions and to be confirmed with thorough investigation. Without further verification, they were not included as lesion ROIs. Values of all pixels within each ROI were averaged for k_{ex}, CEST and MT contrast maps. DWI appeared to delineate different lesion areas than k_{ex} images. Therefore, the lesion ROIs were separately manually drawn on the DWI images and then the areas of infarct lesions both in k_{ex} and DWI were compared. To summarize CEST or MT contrast at different B_1s, the percentage changes of the CEST or MT contrast from ischemic tissues compared to contralateral tissues were also computed as 100% × (Lesion – Control)/Control.

2.4 Statistical analysis

Two-tailed paired Student's t-tests were used to compare parameters (k_{ex}, CEST and MT) between ischemic lesions and contralateral normal tissues for the whole patient group. The value of parameters were presented as mean ± standard deviation. $P < 0.05$ was considered statistically significant. Statistical analysis was performed using Statistical Product and Service Solutions (SPSS, version 19.0, Chicago, IL) software.

3 Results

Fig. 1a demonstrates Z-spectra data from infarct brain tissues at different saturation B_1s. Z-spectrum was fitted for direct saturation (Fig. 1b) and DS-removed residual signal was used to construct omega plots and quantify k_{ex} for all pixels from lesions or control tissues as demonstrated in Fig. 1c. k_{ex} map from a representative subject is shown in Fig. 2. Infarct lesion was clearly delineated in the k_{ex} map with a remarkably elevated signal. Compared to contralateral normal tissues, k_{ex} from lesions increased significantly ($893 \pm 52\ s^{-1}$ vs. $739 \pm 34\ s^{-1}$, $P < 0.001$, Fig. 2c). As shown in Fig. 3, infarct lesions typically showed larger areas in k_{ex} maps than they were in DWI images. Quantitatively, the areas of lesions increased

with different degrees (from 3.69% to 297%, mean and standard deviation 43.6 ± 67.7%, $P < 0.05$) in k_{ex} maps compared to that delineated in DWI images for all patients.

In Fig. 4, a representative k_{ex} map was compared with conventional CEST and MT contrast maps. While the k_{ex} map clearly define lesions from control tissues, the signals of lesions varied greatly with B_1 in CEST and MT maps (Fig. 4d-i). At $B_1 = 1.5$ μT, compared with contralateral healthy tissues, CEST signals of lesions were reduced, however, they were increased at 2.5 or 3.5 μT. No statistically significant difference was shown between infarcts and contralateral tissues ($P > 0.05$) for CEST in any B_1 due to large standard deviations (Fig. 5a, b). On the other hand, MT values of lesions were consistently reduced under varying B_1s (Fig. 5c, d).

4 Discussion and Conclusions

In the present study, we have successfully implemented k_{ex} MRI for clinical patients with ischemic stroke. By comparing to other conventional MRI contrasts, we have investigated k_{ex} as a novel and unique contrast for the delineation of infarct lesions in human brain.

The k_{ex} maps were derived from the DS-removed Z-spectral signals using the improved omega plot method according to the previous study[8]. Since omega plots are linear functions, at least two Z-spectra collected with different RF saturation B_1s are needed. Under different B_1s, varied exchanging proton species with CEST, NOE, or MT effects were selected. For example, amide proton transfer (APT) CEST effect is optimally saturated under low B_1 around 1 to 2 μT due to the relatively slow amide proton exchange rate[16]. Glutamate CEST effect, on the other hand, is optimal under high saturation powers, for instance $B_1 \geq 3$ μT, given the relatively fast amine proton exchange rate in glutamate[17]. That is to say, the metric of tissue k_{ex} as a general physical parameter is the weighted average for all exchangeable proton species in tissues.

Furthermore, the calculation of k_{ex} from the omega plot is based on the X-intercept of the plot, which depends on the B_1 values of the RF saturation pulse. One can mathematically calculate the influence of B_1 inhomogeneity. A dB_1 inhomogeneity in the pulse strength shifts the omega plot and its X-axis intercept with the amount

$$d\left(\frac{1}{\omega_1^2}\right) = -\frac{2d\omega_1}{\omega_1^3} \tag{5}$$

where $\omega_1 = \gamma B_1$. As a result, the inaccuracy in the calculated exchange rate equal to

$$dk_{ex} = -\left(\frac{k_{ex}}{2\pi\gamma B_1}\right)^3 2\pi\gamma dB_1 \tag{6}$$

This means 5% of B_1 variation will lead to ~7% of k_{ex} deviation when k_{ex} is 800 s^{-1}, indicating the importance of a homogenous RF field. It is also worth mentioning that the omega plot is not sensitive to tissue relaxation times (T_1 and T_2) given that those relaxation times are not part of the X-intercept of the omega plot as shown in Equation 1.

Based on our understanding, tissue k_{ex} could be influenced by pH, temperature, the profile of tissue metabolites containing slow or fast exchangeable protons, or reactive oxygen species (ROS)[8,18]. Following ischemic stroke, increased anaerobic metabolism will lead to tissue acidosis and hence pH reduction in ischemic tissues. Given that proton exchange is base catalyzed around physiological pH, k_{ex} is expected to decrease due to acidosis[7]. In addition, brain temperature is generally well controlled and stable. Particularly, Karaszewski et al. demonstrated that the temperature of ischemic brain tissues changed within 1 °C[19]. Besides pH and temperature, the increase of the concentration of small metabolites with relatively fast proton exchange rate may lead to increase in the overall tissue k_{ex} in infarct lesions. It was reported that some small metabolites, such as excitatory amino acids (glutamate and aspartate) and inhibitory amino acids (GABA and taurine), elevate during the initial stage of stroke (< 24 hours)[20-22]. However, the majority of small metabolites with generally higher exchanging protons decreases after 24 hours[23,24]. Since all of our measurements in this study were performed after 24 hours, the reduction in small metabolites with a relatively faster proton exchange rate compared to macromolecules will likely reduce the observed tissue k_{ex}. The fact that we observed elevated k_{ex} in the infarct lesions eliminates pH, temperature, and the metabolite change as the major factors for the k_{ex} changes due to ischemic stroke.

Our recent studies have discovered that ROS can uniquely and sensitively enhance tissue k_{ex}[18]. In stroke, cerebral ischemia is accompanied by the imbalance between the production of ROS and the antioxidant capacity, which leads to excessive ROS production directly or indirectly involved in oxidative damage to lipids, proteins, and nucleic acids, etc., resulting in cellular damage and death[25]. In addition, the complex metabolic changes including anaerobic metabolism, metabolite profile and oxidative stress are mainly induced in the acute ischemic stroke, however, ROS production is further stimulated by the reperfusion after acute stage[26,27]. Hence, the significantly elevated k_{ex} of the infarct regions in the present study may due to the elevated ROS production. The hypothesis needs further investigation with invasive measurements of tissue ROS in ischemic animal models.

It is interesting also to note that the infarct areas in k_{ex} maps were generally larger than they were in DWI images, indicating that k_{ex} imaging is unique from diffusion MRI for the definition of infarct lesions. This is likely due to the distinctive contrast mechanism between these two techniques. In stroke clinics, the definition of ischemic penumbra can potentially help with the decision of recanalization therapy. Whether this mismatch may help to define ischemic penumbra remains to be investigated with the aid of longitudinal and histological studies.

We observed that CEST and MT contrast maps for the definition of infarct lesions varied with saturation amplitude B_1. CEST of lesions were less than control brain tissues at 1.5 μT, consistent to previous studies with relatively low B_1s(<1.5 μT)[7,28,29]. But, with the saturation powers of 2.5 or 3.5 μT, CEST of lesions were increased to be higher than contralateral tissues. Zhao et al.[30] also reported similar variations of the CEST contrast in infarcted tissues due to varied B_1. On the other hand, although MT was significantly lower in lesions compared to contralateral tissues, its percentage changes were different under

varying B_1s. k_{ex} MRI reflects a physical parameter and has been shown here to be independent and differentiable from conventional CEST and MT MRI contrasts.

With recent advances[31,32], magnetic resonance spectroscopy imaging (MRSI) may be used for high-resolution 3-D imaging of brain metabolites with enhanced clinical translatability. Compared to MRSI, molecular CEST MRI is sensitive to a different set of metabolites given to its unique signaling mechanism. For instance, glutamate and glutamine show as one complex peak in MRS while CEST MRI can only detect glutamate in regular MRI settings. The combination of MRS and CEST methods may help to quantify both. Similarly, creatine and phosphorous creatine have different presentations in MRS and CEST MRI. k_{ex} MRI as a derivative from CEST technique has been found to be sensitive to tissue microenvironment, such as pH and ROS; both are currently not detectable with ‘H-MRS or MRSI.

While the present study has successfully demonstrated the implementation of k_{ex} MRI for ischemic stroke patients, limitations are listed as follows. First, the scanning time may be a concern. It took close to 10 minutes in this study to acquire the entire three sets of Z-spectra for k_{ex} mapping of a single slice. However, since omega plots are linear functions, the total scanning time may be greatly reduced by using only two Z-spectra, and further reduced by decreasing the number of saturation offsets in each Z-spectrum[8]. Second, the 1.5 seconds saturation duration that we used in our data collection is not optimal for reaching steady state; however, due to the tissue’s specific absorption rate (SAR) limits in clinical settings, relatively short duration is preferred. According to simulations with Bloch-McConnell equations, 1.5 seconds of saturation can still achieve around 65% of the steady state saturation when B_1 is 1μT and 99% of the steady state value when B_1 is 4μT for the k_{ex} in the 30 to 3000 s^{-1} range[8]. Third, it is a limitation of the present study that there is a lack of an automatic and objective algorithm for lesion ROI delineation from DWI and k_{ex} images. Finally, the sample size used in this preliminary study is relatively small. Larger sample sizes at different stages of stroke would enhance the characterization of stroke progression. Future longitudinal studies will help to delineate temporal evolvement of tissue k_{ex} post infarction.

In conclusion, we have demonstrated the implementation of k_{ex} MRI for assessing ischemic stroke patients. The utility of this novel and independent contrast may lead to a new perspective on stroke diagnosis and management.

Acknowledgements

This work was supported by the National Natural Science Foundation of China (grant numbers 81570462, 81730049 and 81801666), the NIH grants R21 EB023516 (Cai), R01 AG061114 (Tai&Cai), R21 AG053876 (Tai&Cai), the University of Illinois at Chicago Department of Radiology start-up funds (Cai).

References

1. Li L, Jiang Q, Ding G, et al. MRI identification of white matter reorganization enhanced by erythropoietin treatment in a rat model of focal ischemia. Stroke. 2009;40:936–941. [PubMed: 19150870]
2. Urbanski M, Thiebaut DSM, Rodrigo S, et al. DTI-MR tractography of white matter damage in stroke patients with neglect. Exp Brain Res. 2011;208:491–505. [PubMed: 21113581]

3. Fung SH, Roccatagliata L, Gonzalez RG, et al. MR diffusion imaging in ischemic stroke. Neuroimaging Clin NAm. 2011;21:345–377.
4. Zhang S, Zhu W, Zhang Y, et al. Diffusional kurtosis imaging in evaluating the secondary change of corticospinal tract after unilateral cerebral infarction. Am J Transl Res. 2017;9:1426–1434. [PubMed: 28386368]
5. Sun PZ, Cheung JS, Wang E, et al. Association between pH-weighted endogenous amide proton chemical exchange saturation transfer MRI and tissue lactic acidosis during acute ischemic stroke. J Cereb Blood Flow Metab. 2011;31:1743–1750. [PubMed: 21386856]
6. Harston GW, Tee YK, Blockley N, et al. Identifying the ischaemic penumbra using pH-weighted magnetic resonance imaging. Brain. 2015;138:36–42. [PubMed: 25564491]
7. Tietze A, Blicher J, Mikkelsen IK, et al. Assessment of ischemic penumbra in patients with hyperacute stroke using amide proton transfer (APT) chemical exchange saturation transfer (CEST) MRI. Nmr Biomed. 2014;27:163–174. [PubMed: 24288260]
8. Shaghaghi M, Chen W, Scotti A, et al. In vivo quantification of proton exchange rate in healthy human brains with omega plot. Quant Imaging Med Surg. 2019;9:1686–1696. [PubMed: 31728312]
9. Zhou J, Tryggestad E, Wen Z, et al. Differentiation between glioma and radiation necrosis using molecular magnetic resonance imaging of endogenous proteins and peptides. Nat Med. 2011;17:130–134. [PubMed: 21170048]
10. Dixon WT, Ren J, Lubag AJ, et al. A concentration-independent method to measure exchange rates in PARACEST agents. Magn Reson Med. 2010;63:625–632. [PubMed: 20187174]
11. McMahon MT, Gilad AA, DeLiso MA, et al. New "multicolor" polypeptide diamagnetic chemical exchange saturation transfer (DIACEST) contrast agents for MRI. Magn Reson Med. 2008;60:803–812. [PubMed: 18816830]
12. Vinogradov E, Sherry AD, Lenkinski RE. CEST: from basic principles to applications, challenges and opportunities. J Magn Reson. 2013;229:155–172. [PubMed: 23273841]
13. Jones CK, Huang A, Xu J, et al. Nuclear Overhauser enhancement (NOE) imaging in the human brain at 7T. Neuroimage. 2013;77:114–124. [PubMed: 23567889]
14. van Zijl PC, Yadav NN. Chemical exchange saturation transfer (CEST): what is in a name and what isn't? Magn Reson Med. 2011;65:927–948. [PubMed: 21337419]
15. Cai K, Singh A, Poptani H, et al. CEST signal at 2ppm (CEST@2ppm) from Z-spectral fitting correlates with creatine distribution in brain tumor. Nmr Biomed. 2015;28:1–8. [PubMed: 25295758]
16. Zhou J, Payen JF, Wilson DA, et al. Using the amide proton signals of intracellular proteins and peptides to detect pH effects in MRI. Nat Med. 2003;9:1085–1090. [PubMed: 12872167]
17. Cai K, Haris M, Singh A, et al. Magnetic resonance imaging of glutamate. Nat Med. 2012;18:302–306. [PubMed: 22270722]
18. Tain RW, Scotti AM, Cai K. Improving the detection specificity of endogenous MRI for reactive oxygen species (ROS). J Magn Reson Imaging. 2019;50:583–591. [PubMed: 30614137]
19. Karaszewski B, Wardlaw JM, Marshall I, et al. Measurement of brain temperature with magnetic resonance spectroscopy in acute ischemic stroke. Ann Neurol. 2006;60:438–446. [PubMed: 16972284]
20. Graham SH, Chen J, Sharp FR, et al. Limiting ischemic injury by inhibition of excitatory amino acid release. J Cereb Blood Flow Metab. 1993;13:88–97. [PubMed: 8093250]
21. Kimberly WT, Wang Y, Pham L, et al. Metabolite profiling identifies a branched chain amino acid signature in acute cardioembolic stroke. Stroke. 2013;44:1389–1395. [PubMed: 23520238]
22. Melani A, Pantoni L, Corsi C, et al. Striatal outflow of adenosine, excitatory amino acids, gamma-aminobutyric acid, and taurine in awake freely moving rats after middle cerebral artery occlusion: correlations with neurological deficit and histopathological damage. Stroke. 1999;30:2448–2454, 2455. [PubMed: 10548683]
23. Pascual JM, Carceller F, Roda JM, et al. Glutamate, glutamine, and GABA as substrates for the neuronal and glial compartments after focal cerebral ischemia in rats. Stroke. 1998;29:1048–1056, 1056–1057. [PubMed: 9596256]
24. Yang M, Wang S, Hao F, et al. NMR analysis of the rat neurochemical changes induced by middle cerebral artery occlusion. Talanta. 2012;88:136–144. [PubMed: 22265479]

25. Chan PH. Reactive oxygen radicals in signaling and damage in the ischemic brain. J Cereb Blood Flow Metab. 2001;21:2–14. [PubMed: 11149664]
26. Brouns R, De Deyn PP. The complexity of neurobiological processes in acute ischemic stroke. Clin NeurolNeurosurg. 2009;111:483–495.
27. Crack PJ, Taylor JM. Reactive oxygen species and the modulation of stroke. Free Radic Biol Med. 2005;38:1433–1444. [PubMed: 15890617]
28. Song G, Li C, Luo X, et al. Evolution of Cerebral Ischemia Assessed by Amide Proton Transfer-Weighted MRI. Front Neurol. 2017;8:67. [PubMed: 28303115]
29. Msayib Y, Harston G, Tee YK, et al. Quantitative CEST imaging of amide proton transfer in acute ischaemic stroke. Neuroimage Clin. 2019;23:101833. [PubMed: 31063943]
30. Zhao X, Wen Z, Huang F, et al. Saturation power dependence of amide proton transfer image contrasts in human brain tumors and strokes at 3 T. Magn Reson Med. 2011;66:1033–1041. [PubMed: 21394783]
31. Lam F, Li Y, Guo R, et al. Ultrafast magnetic resonance spectroscopic imaging using SPICE with learned subspaces. Magn Reson Med. 2020;83:377–390. [PubMed: 31483526]
32. Lam F, Ma C, Clifford B, et al. High-resolution (1) H-MRSI of the brain using SPICE: Data acquisition and image reconstruction. Magn Reson Med. 2016;76:1059–1070. [PubMed: 26509928]

Highlights

- Proton exchange rate (k_{ex}) imaging was proposed based on water direct saturation (DS)-removed omega plots
- k_{ex} MRI can differentiate infarcts from contralateral normal brain tissues
- k_{ex} MRI was different from conventional MRI contrasts

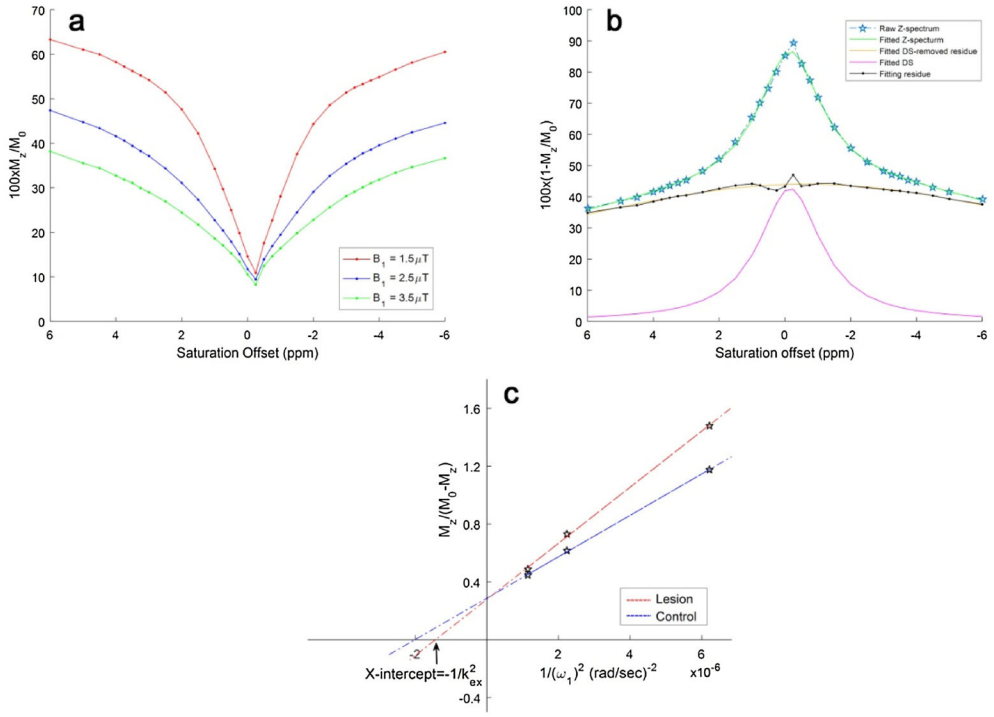

Fig. 1.

Direct saturation removed Omega plots for the quantification of k_{ex}. **a** Typical Z-spectra of infarct brain tissues plotted form −6 to 6 ppm for three different saturation powers B_1s (1.5, 2.5, 3.5 μT). **b** The process of removing water DS by Lorentzian fitting is demonstrated with a Z-spectrum at 1.5 μT. DS was subtracted from the entire Z-spectrum and the residual signals were used for constructing the omega plot. **c** Typical DS-removed omega plots of infarct (red line) and control brain tissue (blue line). The plots were linear, and the X-intercept of the omega plots provided a direct readout of the exchange rates of infarct or healthy brain tissues.

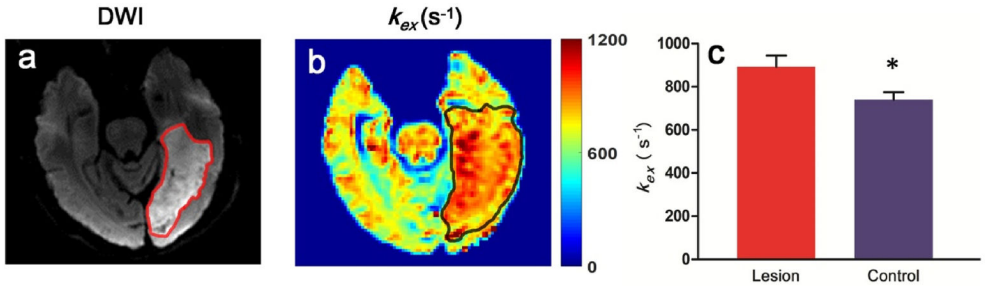

Fig. 2.

k_{ex} map from a representative ischemic stroke patient. **a** DWI exhibited an infarct lesion in the left occipital lobe. **b** k_{ex} map also clearly showed the lesion with an elevated signal. **c** The bar plots showed that k_{ex} of lesions were significantly increased compared with that of the contralateral tissues for all patients. * represents significant differences between infarct lesions and control brain tissues for k_{ex}.

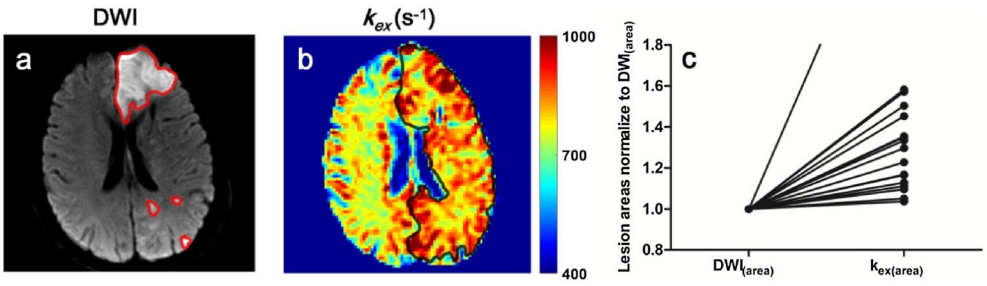

Fig. 3.

A representative case showing that the k_{ex} map defines larger lesion area than DWI. **a** DWI exhibited a massive infarct in the left frontal lobe and scattered small infarcts in the left occipital lobe. The ROI profiles of infarct lesions in DWI image are delineated with red lines. **b** k_{ex} map exhibited increased signal covering the majority of the whole left hemisphere. The ROI profile of infarct lesion in k_{ex} map is delineated with black line. **c** Larger lesion areas in k_{ex} maps ($k_{ex(\text{area})}$) were shown from all individual patients compared to lesion areas delineated with DWI images ($\text{DWI}_{(\text{area})}$, normalized to 1).

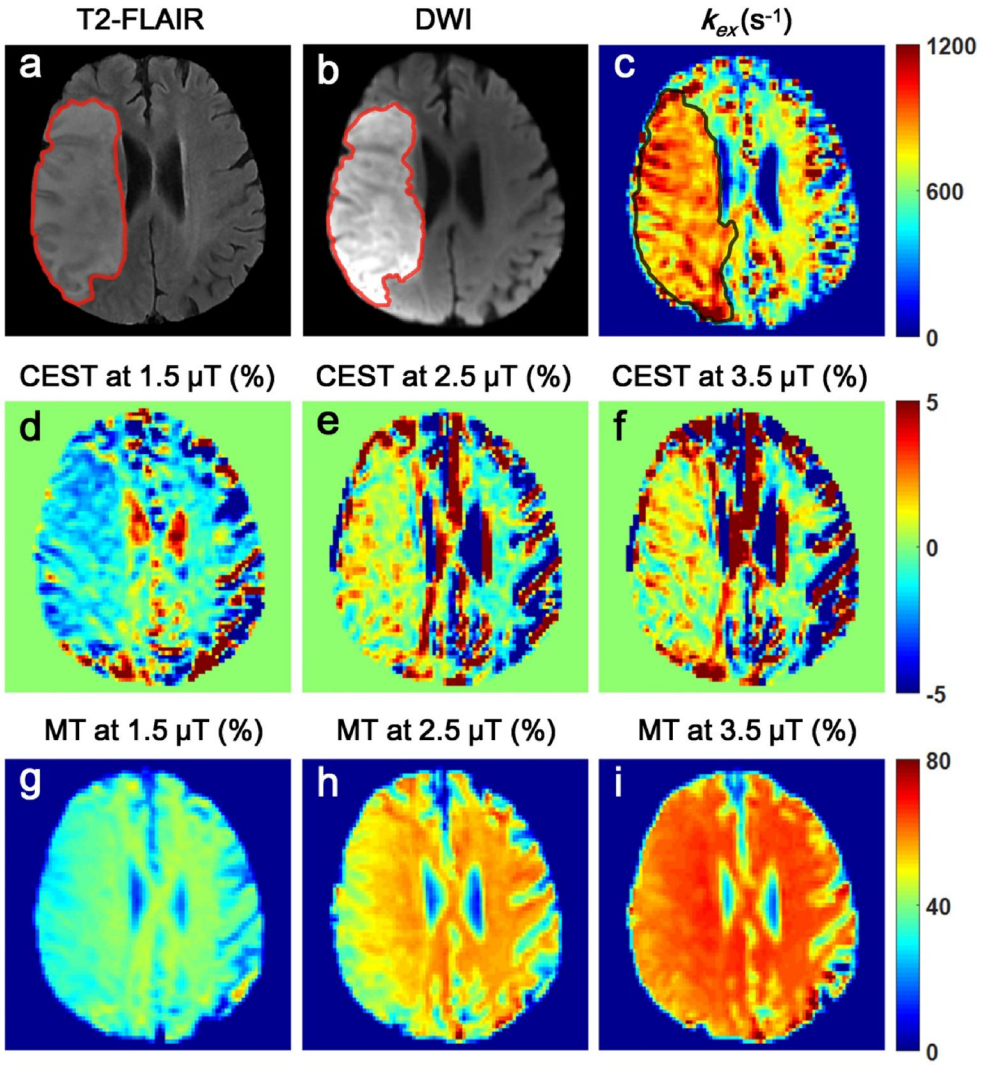

Fig. 4.

The comparison among k_{ex}, CEST and MT maps from a representative patient. **a-c** T2-FLAIR, DWI and k_{ex} maps clearly showed the location and extent of the infarct. **d-i** CEST and MT contrasts of lesions were highly variable with B_1.

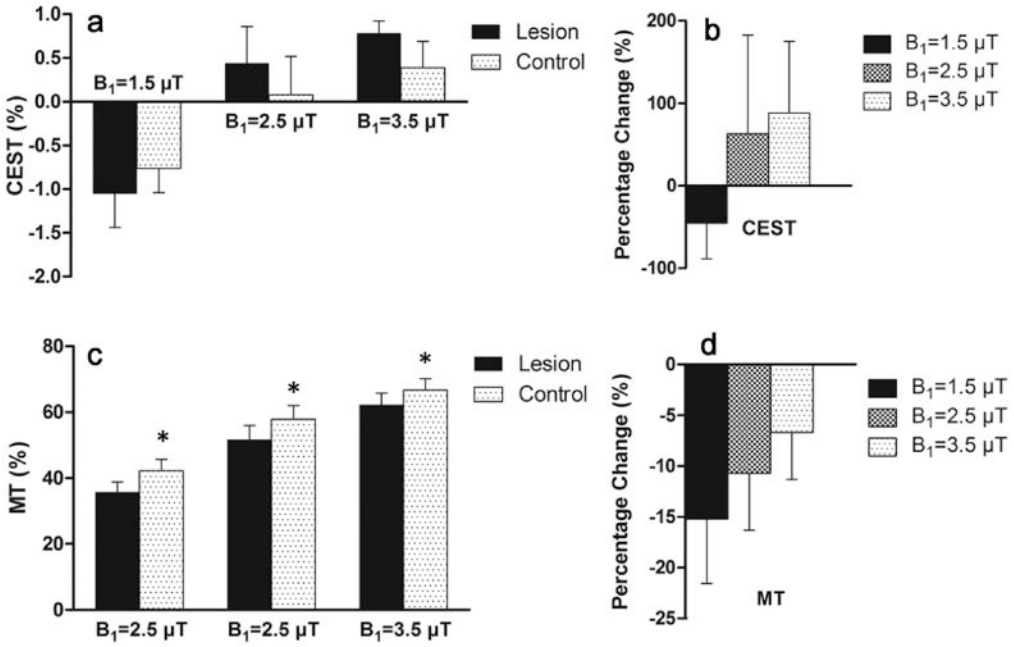

Fig. 5.

CEST/MT contrasts of infarct lesions varied with saturation amplitude B_1. **a** ompared to healthy brain tissues, CEST contrast of lesions was reduced at 1.5 μT, but increased at 2.5 or 3.5 μT, confirmed by the percentage changes between lesions and healthy tissues as shown in Figure **b**. Figure **c** shows MT of lesions was consistently reduced, however, at decreased degrees with higher B_1 as shown in Figure **d**. * represents significant differences ($P < 0.05$) between infarct lesions and control brain tissues for MT.